PHILOSOPHICAL TRANSACTIONS OF THE ROYAL SOCIETY A MATHEMATICAL, PHYSICAL & ENGINEERING SCIENCES

The L3 Experiment

David P. Stickland

Phil. Trans. R. Soc. Lond. A 1991 **336**, 223-236
doi: 10.1098/rsta.1991.0075

The L3 experiment

By David P. Stickland

Department of Physics, Princeton University, Princeton, New Jersey 08544, U.S.A.

The L3 experiment has completed the first two years of data-taking at the LEP e^+e^- collider at CERN. The detectors are contained in a very large solenoidal magnetic field volume, with the emphasis on precision measurement of electrons, photons and muons. The physics goals, design and performance of the detector are reviewed, with highlights from the results that have been obtained during LEP running at the Z^0 resonance.

1. Introduction

LEP provides high-luminosity e^+e^- collisions in the energy range, $\sqrt{s}$, from about 80 GeV to, eventually, about 200 GeV. In 1989 and 1990 LEP has been operated near the Z^0 resonance. L3 is one of the four large experiments at LEP; the physics goals of L3 are: (1) the search for new particles such as the Higgs boson, and (2) performance of precision tests of the Standard Model (Glashow 1961; Salam 1968; Weinberg 1967) at the Z^0 resonance and above the W^+W^- production threshold.

New physics can be found in essentially two ways: firstly by the explicit observation of new particles or interactions, and secondly by the effects of that new physics on precision measurements of parameters of the Standard Model. Historically many of the revolutions in particle physics have been made by precision measurements involving leptons and photons. Examples are: the discovery of the J particle in $pN \rightarrow e^+e^-X$ and the subsequent study of c-quark systems; the discovery of the Y in $pN \rightarrow \mu^+\mu^-X$ and the subsequent study of b-quark systems; the discovery of the Z and W bosons in lepton final states at the CERN $\bar{p}p$ collider.

In all these cases, while the decay rates into hadrons of these particles were much larger than those for leptonic decays, the discovery was via the lepton channel, where signatures are in general much cleaner. The high precision possible with lepton measurements, allows for much better background rejection in searching for new physics.

We have therefore chosen a design which emphasizes the precision measurement of muons in free space and the precise measurement of electron and photon energies in a compact calorimeter made of bismuth germanium oxide (BGO) crystals. Additionally we have instrumented almost 4π coverage with hadron calorimetry to both measure the hadronic energy in the event, and ensure an hermetic detector; which is particularly important at LEP II (above the W^+W^- threshold) where the measurement of missing energy (neutrinos) will be important.

2. The L3 detector

The L3 experiment is the result of an effort involving a worldwide collaboration of almost 500 physicists belonging to 41 institutions in 13 countries. The preparation of the experiment took eight years from its conception to the beginning of data-taking

Phil. Trans. R. Soc. Lond. A (1991) **336**, 223–236
Printed in Great Britain

in 1989. The detectors are installed within a 7800 t magnet providing a 0.5 T field. We chose a relatively large volume to optimize the muon momentum resolution. The detector is described in detail in L3 (1990). From the interaction point outwards, the following detectors are installed (figure 1).

1. A central detector, comprising a time expansion chamber (TEC), which tracks charged particles with approximately 50 μm average single-wire accuracy in the bending plane. In the non-bending plane, the Z coordinates are measured by four layers of additional wire chambers providing 300 μm single track resolution.

2. An electromagnetic calorimeter using BGO crystals, which absorb the electromagnetic energy and give out scintillation light. This detector is capable of 5% accuracy at 100 MeV and 1% above 2 GeV.

3. A hadron calorimeter measuring hadron energies with $(55/\sqrt{E}+5)\%$ resolution. The hadron calorimeter also provides a clean muon sample by absorbing hadrons close to the e^+e^- interaction point, and by tracking the muons through the uranium absorber.

4. A muon detector, comprising large drift chambers able to measure the sagitta of muon tracks to provide a final muon momentum resolution of about 2.5% at 50 GeV, after compensation for the energy lost in the calorimeters.

5. A luminosity monitor measuring the small angle Bhabha scattering rate with an experimental precision of better than 1%.

The detectors are complemented by triggering and data taking electronics, a cluster of online computers, a mainframe computer for offline event reconstruction and a workstation cluster for physics analysis.

In the following subsections the main features of each detector element are described, and examples given from the physics results to illustrate the performance.

2.1. *The precision muon spectrometer*

The design goals of the muon spectrometer are to identify muons over a large solid-angle; to measure muon momentum with high accuracy; to reconstruct dimuon mass with high precision.

This has been achieved using a configuration of three layers of drift chambers which very precisely measure the curvature of the muon trajectory in the region between the hadron calorimeter and the magnet coil. In this region a 50 GeV muon deviates from a straight line with a sagitta of $s = 3.4$ mm. To obtain good dimuon mass resolution we require that the direction of the muons is measured in the central tracking chamber, and the sagitta (momentum) is measured in the muon chambers with a precision of $\Delta s/s \approx 2\%$, i.e. 70 μm.

The muon detector is modular, comprising two ferris wheels each having eight octants, the chambers in the two ferris wheels are electrically connected such that the detector appears to have simple octagonal symmetry. The total volume occupied is some 1000 m^3. The detector has been designed to minimize the contributions from the major causes of error in the sagitta measurements which are (*a*) intrinsic resolution of the drift chambers; (*b*) multiple scattering; (*c*) accuracy of alignment of chambers belonging to different layers.

A muon track traversing the whole muon system passes a total of 56 wires, such that an intrinsic accuracy of 250 μm per wire is sufficient to reach the design resolution. Thin aluminium honeycomb with an average radiation length of 0.9% per two layers is used to enclose the middle chambers, whereby the multiple scattering induced sagitta error is kept below 30 μm. Finally, muons above 3 GeV pre-

PHILOSOPHICAL TRANSACTIONS OF THE ROYAL SOCIETY A MATHEMATICAL, PHYSICAL & ENGINEERING SCIENCES

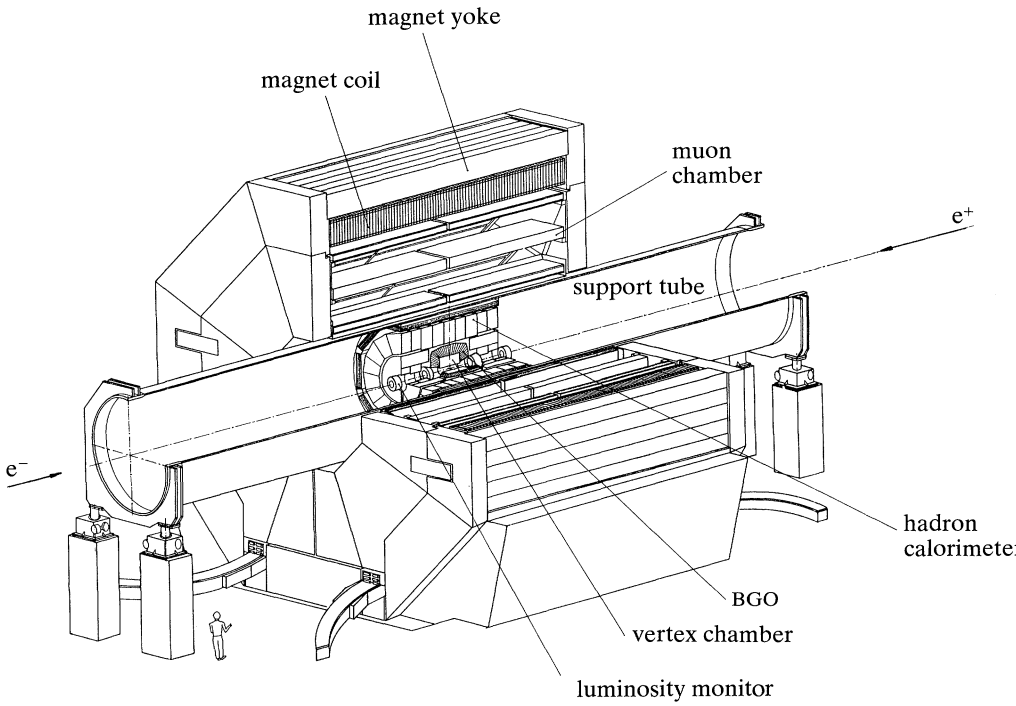

Figure 1. A schematic view of the L3 detector.

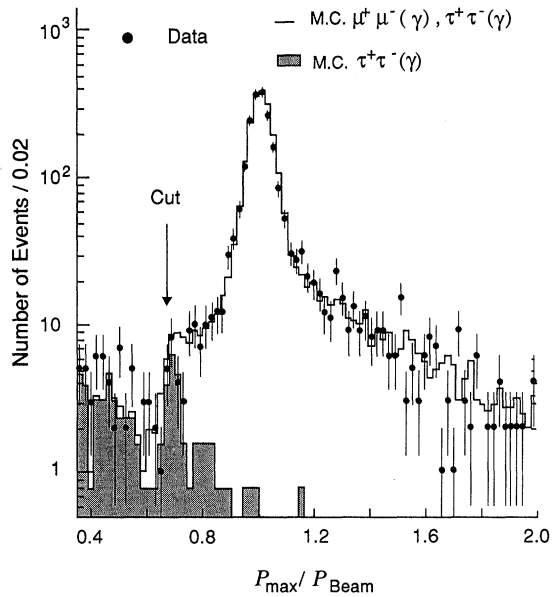

Figure 2. Distribution of the maximum muon momentum in the $e^+e^- \to \mu^+\mu^-(\gamma)$ events at the Z^0 peak compared with the Monte Carlo simulation, including the simulation of the $e^+e^- \to \tau^+\tau^-(\gamma)$ background.

dominantly stay inside one octant, therefore precision alignment is only necessary within one octant. By the use of complex optical and mechanical measurements this is also such that the induced sagitta error from alignment errors is below 30 μm.

To reconstruct the momentum of the muon at the vertex, the muon is backtracked through the uranium of the hadron calorimeter to determine the most probably energy loss for such a muon trajectory, which is then added to the momentum measured in the muon chambers. By comparing the expected energy loss with that observed in the hadron calorimeter, we obtain additional sensitivity to remove muons from decays and punch-through. The tracking information from the central tracking chamber can be used to improve the knowledge of the muons initial direction.

In figure 2 the experimental resolution of the muon chambers is illustrated with 45 GeV muons from Z^0 decay. The data and simulation are in good agreement. The momentum resolution for tracks measured in three muon chambers, is between 2.5 and 3% depending on the octant number. (This variation has been understood to be due to data-acquisition problems which have been corrected for the 1991 data-taking period.)

2.2. *Electron and photon measurement*

The electromagnetic calorimeter uses bismuth germanate (BGO) crystals as both the showering and the detecting medium. BGO has a high stopping power (short radiation length) for electrons and photons, which make it particularly attractive as an electromagnetic calorimeter. For the 1989 and 1990 data-taking periods the coverage was for polar angle θ in the range $42° < \theta < 138°$. In preparation for the 1991 run, endcaps were added extending the coverage down to $12° < \theta < 168°$; however, for all results presented here, only the barrel part was in operation.

The calorimeter consists of about 11 000 BGO crystals pointing to the interaction region. Each crystal is 24 cm long and is a truncated pyramid about 2×2 cm^2 at the entrance and 3×3 cm^2 at the outer end. The scintillation light is detected by silicon photodiodes. An electromagnetic shower from a 50 GeV electron leaves about 70% of its energy in one crystal and more than 98% of its energy in a 5×5 crystal matrix around the central crystal. The calibration of such a device is crucial, all the crystals were calibrated at three different electron energies from 2 to 50 GeV and using cosmic rays. From test beam studies we have determined that the energy resolution is approximately 5% at 100 MeV falling to less than 1% above a few GeV.

This performance has been confirmed at LEP, the measured energy resolution averaged over the whole calorimeter for 45 GeV electrons from Bhabha scattering is 1.2% in perfect agreement with the predictions of the Monte Carlo taking into account detector resolution and initial and final state radiation. It is more difficult to determine the *in situ* low-energy performance, since we do not have a line source of electrons or photons at low energy. However, we have studied π^0 and η particles identified by their $\gamma\gamma$ decays in hadronic events. In figure 3 we show the invariant mass spectra of $\gamma\gamma$ combinations near the π^0 and η masses. The measured widths are in good agreement with the predictions of the Monte Carlo, indicating that the low-energy performance of the detector is also as designed.

2.3. *Hadron calorimetry*

Hadron energies are measured in the BGO and hadron calorimeters (HCAL). Because the nuclear interaction length of BGO is small (22 cm) many hadronic showers start to form in the BGO. The remaining energy is absorbed in a fine sampling calorimeter

PHILOSOPHICAL TRANSACTIONS OF THE ROYAL SOCIETY A MATHEMATICAL, PHYSICAL & ENGINEERING SCIENCES

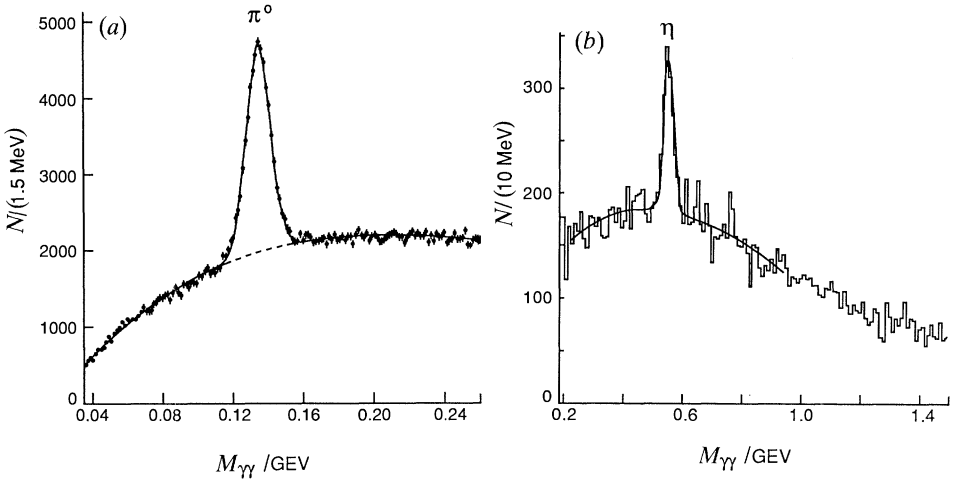

Figure 3. The invariant mass spectrum for γγ combinations in the region of (*a*) the π^0 and (*b*) the η. (*a*) $\sigma = 7$ MeV, (*b*) $\sigma = 18$ MeV.

made of uranium plates interspersed with proportional wire chambers. The HCAL acts both as an energy measuring device and as a filter for the muons; there are approximately six nuclear interaction lengths of material between the vertex and the muon chambers.

The HCAL has two basic units, the barrel and endcap. While there are geometric and readout differences between the two units, the basic principles are the same. For simplicity only the barrel part is described here. The HCAL barrel modules are arranged in nine rings arranged longitudinally around the beampipe. Each ring is constructed from 16 modules, within each module the proportional chambers are arranged to give alternately readout in the azimuthal and the longitudinal directions. There are about 300000 proportional wires in the system but these are grouped together to give 23040 readout channels.

The natural radiation in the uranium is used to give a relative calibration of the HCAL cells. The absolute calibration is most easily determined by fitting the total observed energy distribution in BGO and HCAL modules for hadronic Z^0 events, in such a way as to minimize the total energy resolution. In this way the best weighting factors with which to add together BGO and HCAL information are determined. (Adriani *et al.* 1990). The result of these fits is shown in figure 4 comparing Monte Carlo predictions for the total energy measurement with the data. The measured resolution is in good agreement with the previously obtained test beam result of $(55/\sqrt{E}+5)\%$.

2.4. *The central tracking chamber*

The central tracking chamber is designed with the following goals: (i) detection of charged particles and measurement of their locations and directions; (ii) determination of the transverse momentum and sign of the charge for particles up to 50 GeV; (iii) reconstruction of the impact point and direction for charged particles at the entrance to the electromagnetic calorimeter; (iv) reconstruction of the interaction point and of secondary vertices for particles with a lifetime greater than 10^{-13} s.

The constraints imposed on the detector are considerable, the inner radius of the BGO limits the lever arm to 37 cm and the size of the magnet limits the magnetic field

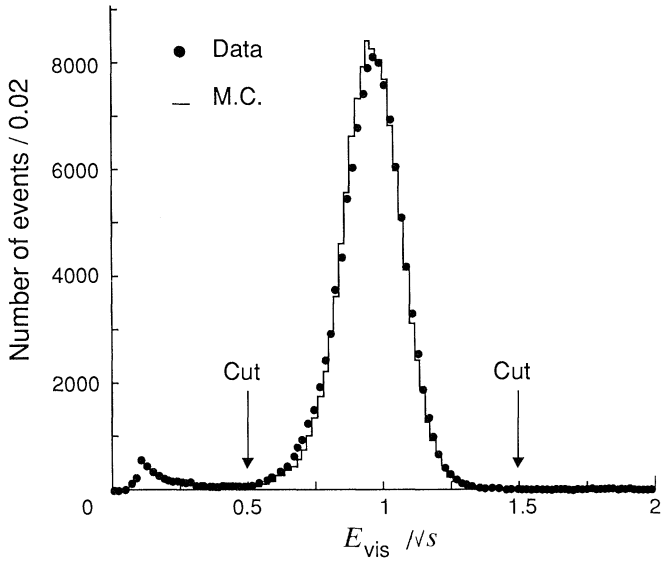

Figure 4. The total energy distribution for hadronic events. Also shown is the prediction of the Monte Carlo. The energy resolution for hadron events is approximately 10.5% (with some dependence on polar angle).

to 0.5 T. Thus to measure the charge of a 50 GeV track requires 50 coordinate measurements per track with a single wire precision of better than 50 μm. This is accomplished by two concentric cylindrical drift chambers on common endplates operated in a 'time expansion' mode (TEC).

Following the TEC principle, the high field amplification region at the sense plane is separated from the low drift field region by an additional grid wire plane. At the present stage an average single wire resolution of 58 μm has been obtained. This has been determined from the residual distributions for $\mu^+\mu^-$ events.

In the B-physics discussed below, the electron sample has been selected requiring, among other things a matching between the track and the energy cluster in the BGO. A charge confusion of better than 1% has been obtained. We have also used the sample of $b\bar{b}$ events to measure the B-hadron lifetime using the impact parameter method (L3 1991). Figure 5 shows the signed impact parameter distribution from which we derive a value of $\tau_B = 1.32 \pm 0.08\,(stat) \pm 0.09\,(sys)$, this measurement being compatible with and having errors comparable to the previously existing world average.

2.5. *The measurement of luminosity*

The luminosity monitor consists of two electromagnetic calorimeters and two sets of proportional wire chambers situated symmetrically on either side of the interaction point. Each calorimeter is a finely segmented and azimuthally symmetric array of 304 BGO crystals covering the polar angular range $24.93 < \theta$ or $(\pi - \theta) < 69.94$ mrad. The Bhabha scattering cross section, $e^+e^- \to e^+e^-(\gamma)$, can be precisely calculated at second order in α. The visible cross section in the luminosity monitor after all cuts is 88.5 nb, almost three times larger than the $Z^0 \to q\bar{q}$ cross section at the Z^0 resonance.

Two separate samples of Bhabha events are maintained. In the first (second) sample, a tight fiducial volume cut is imposed on the calorimeter on the $+z$ ($-z$) side.

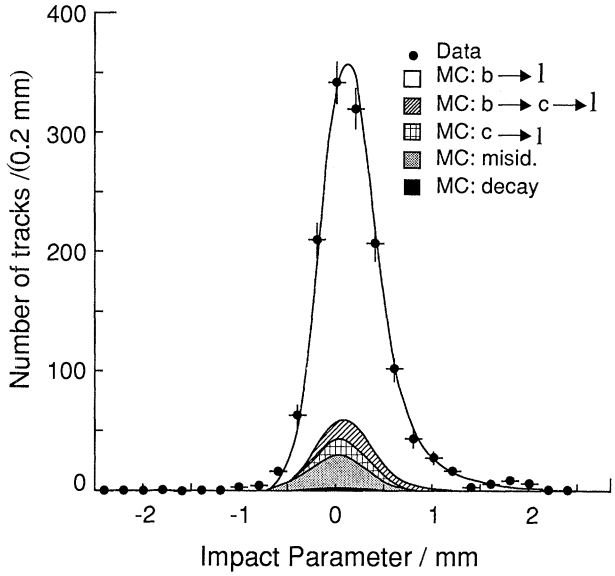

Figure 5. The signed impact parameter of lepton tracks in B-hadron decays. The solid line is a best fit curve to the resolution function of the TEC and the B-hadron lifetime. The distribution shows a clear bias to positive impact parameters, as expected for particles with a small, but measurable, lifetime.

The selection of Bhabha events depend on three criteria: (i) a fiducial volume cut well within one of the calorimeters; (ii) energy cuts for the electron candidates; (iii) a coplanarity cut between the two electron candidates.

By using the average of the two Bhabha samples, the asymmetric fiducial volume cuts greatly reduce the systematic effect on the luminosity measurement due to calorimeter misalignments and/or e^+e^- interaction point displacements. The total systematic error we estimate for the luminosity measurement is 0.7% coming from the experimental systematics and 0.5% arising from theoretical systematic uncertainties.

In figure 6 we show the polar angle distribution for the Bhabha scattering candidates. Of particular importance is the excellent agreement at the inner edge of the calorimeter where the cross section is rising steeply.

3. Physics highlights

3.1. *The Z^0 lineshape*

In 1989 after one month of LEP running, and with a sample of 2538 hadronic Z^0 decays, we published our first results on the Z^0 lineshape (L3 1989). The error on the mass then obtained was 57 MeV. In 1990 using a total luminosity of 5.5 pb^{-1}, corresponding to approximately 115000 hadronic and 10000 leptonic Z^0 decays, we have been able to make very precise measurements of the Z^0 mass and couplings (L3 1991*a*).

From a simultaneous fit to all of our measured cross-section data, we obtain assuming lepton universality:

$$M_Z = 91.181 \pm 0.010 \pm 0.02\ (\text{LEP})\ \text{GeV}, \quad \Gamma_Z = 2501 \pm 17\ \text{MeV},$$
$$\Gamma_{\text{had}} = 1742 \pm 19\ \text{MeV}, \quad \Gamma_l = 83.6 \pm 0.8\ \text{MeV}.$$

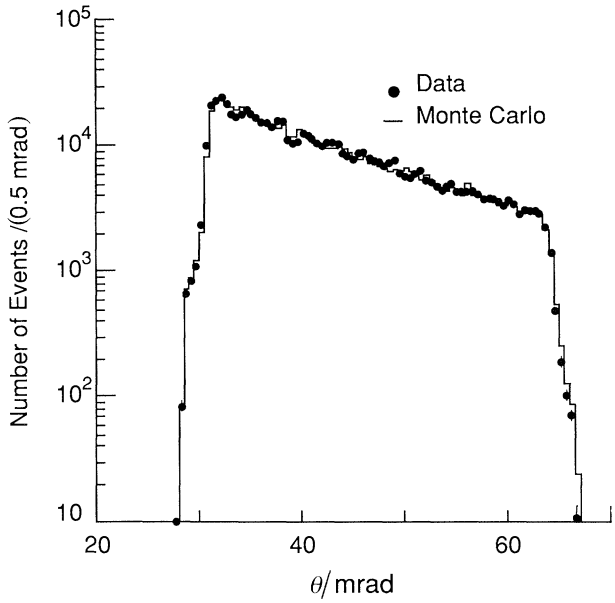

Figure 6. The distribution of the observed polar scattering angle, θ. The wiggles in the distribution are due to the changing angular resolution across the face of each crystal. The solid line shows the Monte Carlo simulation.

If we do not assume lepton universality, we obtain for the partial decay widths of the Z^0 into e^+e^-, $\mu^+\mu^-$ and $\tau^+\tau^-$:

$$\Gamma_e = 83.3 \pm 1.1\,\text{MeV}, \quad \Gamma_\mu = 84.5 \pm 2.0\,\text{MeV}, \quad \Gamma_\tau = 84.0 \pm 2.7\,\text{MeV}.$$

From the measured ratio of the invisible and the leptonic decay widths of the Z^0, we determine the number of light neutrino species to be $N_\nu = 3.05 \pm 0.10$.

Including our measurements of the forward-backward asymmetry for the leptonic channels in a fit to determine the vector and axial-vector neutral current coupling constants of charged leptons to the Z^0, we obtain $\bar{g}_v = -0.046^{+0.015}_{-0.012}$ and $\bar{g}_a = -0.500 \pm 0.003$. In the framework of the Standard Model, we estimate the top quark mass to be $m_t = 193^{+52}_{-69} \pm 16$ (Higgs) GeV, and we derive a value for the weak mixing angle of $\sin^2\theta_W \equiv 1-(M_W/M_Z)^2 = 0.222 \pm 0.008$, corresponding to an effective weak mixing angle of $\sin^2\bar{\theta}_W = 0.2315 \pm 0.0025$.

To illustrate the remarkable quality of the data we show in figure 7 the measured and fitted cross sections.

3.2. *Searches for the Higgs particle*

We have performed searches for the neutral Higgs boson (Higgs 1964 *a*, *b*, 1966; Englert & Brout 1964) in our data. The $e^+e^- \to Z^0 \to H^0 + Z^{0*}$ cross section is predicted by the Standard Model and depends on the Higgs mass (Berends & Kleiss 1985). The Higgs decay partial widths into fermions are also well-established for masses of the H^0 greater than 2 GeV (Franzini *et al.* 1989). Below 2 GeV non-perturbative effects make the prediction of the branching ratios of the Higgs boson decaying into hadrons and leptons less firm, for this reason in the low mass search we follow no particular model but make an independent search for each Higgs decay channel.

The rate for the Z^{0*} decay to neutrinos is much larger than to leptons, so for high

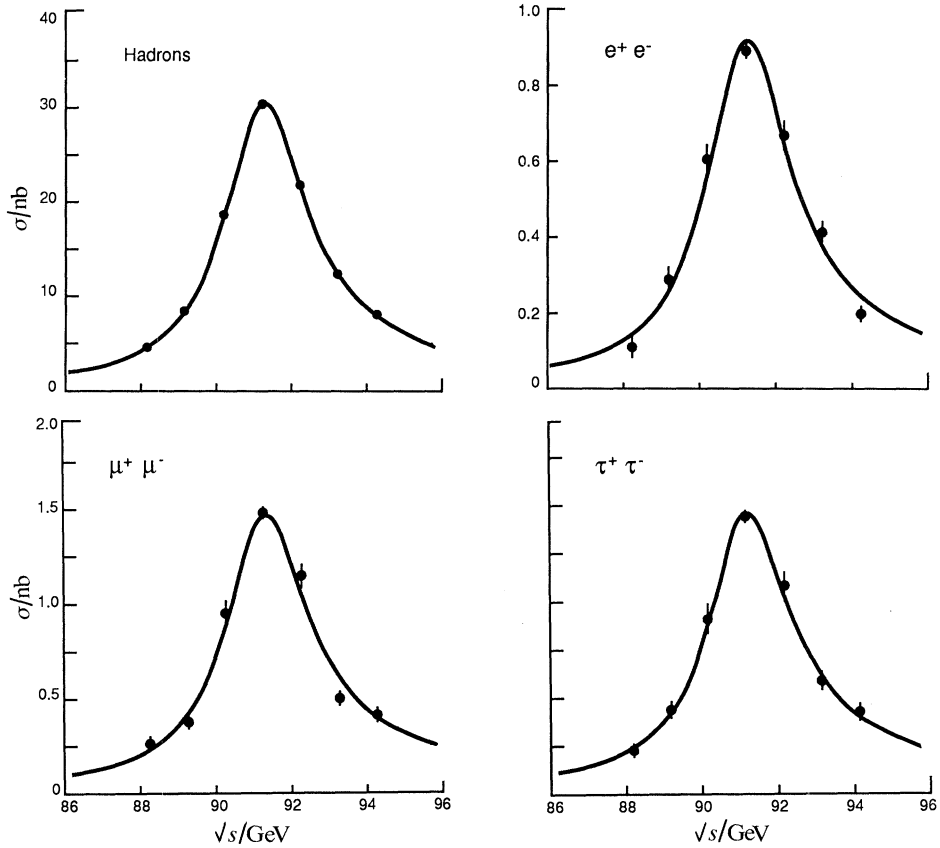

Figure 7. The cross sections for $e^+e^- \to$ hadrons, e^+e^-, $\mu^+\mu^-$, $\tau^+\tau^-$ as a function of $\sqrt{s}$. In all cases the cross sections are corrected for geometrical acceptance. For the case of $e^+e^- \to e^+e^-$ only the s-channel cross section in the angular range $44° < \theta < 136°$ and with the acollinearity angle between the electron candidates, $\zeta < 25°$, is shown. The solid curves are the result of the Standard Model fit to the hadronic and leptonic cross-section measurements.

mass Higgs particles the most sensitive search channel is $H^0 \to b\bar{b}$ with $Z^{0*} \to \nu\bar{\nu}$. In figure 8 we show the expected numbers of events as a function of Higgs mass, since no events were observed we are able to set the limit as indicated. The results of our searches are given in L3 (1990 *a*, b, 1991 *b*). We exclude at the 95% confidence level the existence of a standard neutral Higgs particle with a mass in the range $0 < M_H < 41.8$ GeV. (The limits at low mass are actually at greater than 99% confidence level.)

We have also searched, unsuccessfully, for many other particles such as supersymmetric partners to the standard particles, heavy leptons, excited leptons, etc. (L3 1989*a*, 1990*c–g*, 1991*c–d*).

3.3. B *physics*

Approximately 16% of all Z^0 decays give rise to b-quarks. This large fraction makes the Z^0 resonance an ideal place at which to study b-quarks and hadrons carrying a b-quark. The average lifetime of a B-hadron is about 10^{-12} s; this is long enough to be measured using impact parameter methods, but the decays of the B-hadrons occur within the beam pipe so that only the decay products can be directly studied at LEP.

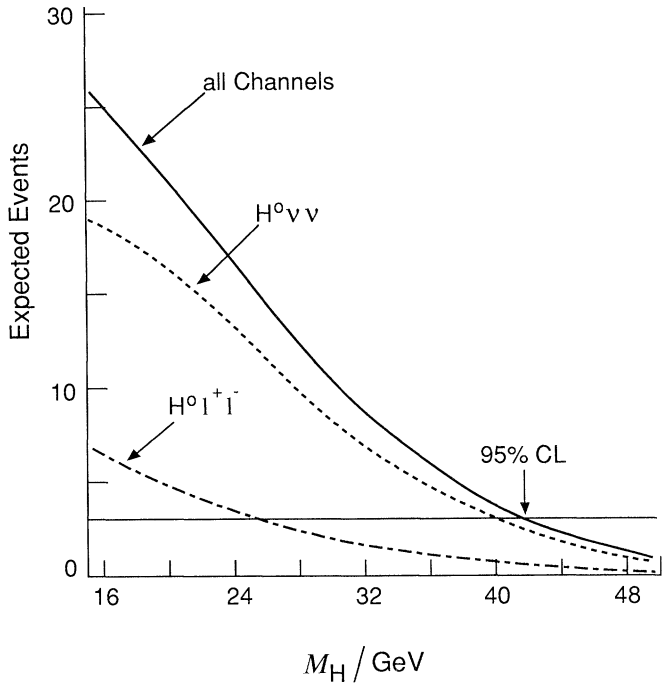

Figure 8. The total number of events expected in the different $H^0 + Z^{0*}$ decay channels. The mass limit corresponding to the 95% confidence level is indicated.

The branching ratio of the b-quark to leptons is about 10% (for electrons and muons). Since the b-quark is typically carrying most of the available energy, the decay lepton typically has high momentum. In the B-hadron decay a jet of particles is normally produced, however, the lepton typically has a momentum transverse to this jet direction of order $p_\perp \approx \frac{1}{4} m_b$. Thus, a sample of events enriched in leptons from the b-quark decay can be selected by requiring that the leptons have both high momentum and high momentum transverse to the nearest jet. Additionally, since the charge of the lepton reflects the charge of the parent b (or $\bar{b}$), it can be used to measure the angular distribution of the $Z^0 \to b\bar{b}$ production. With sufficient statistics, this forms a very precise test of the Standard Model in that it measures with high precision the electron vector coupling to the Z^0, and hence $\sin^2 \theta_W$.

The fraction of real $b \to l$ events in our sample, as evaluated from Monte Carlo studies, is typically 80%. This is illustrated in figure 9.

A complication in the measurement of the forward–backward asymmetry A_b, is that the presence of oscillations between B^0 and $\bar{B}^0$ mesons results in the switching of the sign of the b-quark before its decay, and hence the wrong labelling of the quark charge. This oscillation occurs for B^0-mesons via a second-order weak interaction, in the same way as the well-known mixing of K^0-mesons. Thus it is necessary to measure the strength of mixing for B-mesons in our sample; B^0–$\bar{B}^0$ mixing has been measured previously (UA1 1987; ARGUS 1987; CLEO 1989). The average mixing parameter χ_B is sensitive to the exact mix of mesons available to a given experiment since the separate mixing parameters for B_d^0 and B_s^0 mesons are expected to be very different ($\chi_d \approx 0.15$ and $\chi_s \approx 0.5$ respectively). At the Υ (4S), where CLEO and ARGUS have made their measurements, no B_s^0 mesons are produced, while at LEP 40% of all B^0

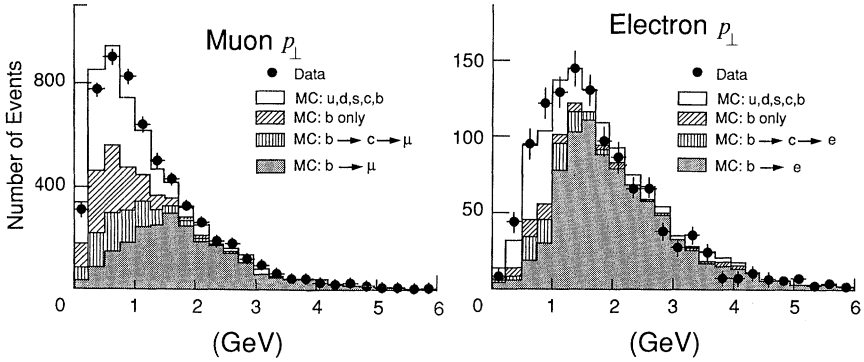

Figure 9. The measured distributions of the transverse momentum $p_\perp$ of the muon (*a*) and electron (*b*) with respect to the nearest jet. Cuts of $P_\mu > 4$ GeV for the muons and $P_e > 3$ GeV for the electrons have been applied. The contributions of the various processes are indicated. The data at large $p_\perp$ are dominated by b→l decays.

mesons are expected to be B_s^0, so we must measure the B^0–B^0 mixing parameter χ_B at LEP. Using events in which both B mesons have decayed semi-leptonically, and comparing the number of same-sign and opposite-sign lepton pairs in those events, we have determined χ_B. We obtain (L3 1990*h*), $\chi_B = 0.178^{+0.049}_{-0.040}$ (stat) ± 0.02 (sys) a result which is consistent with maximal mixing in the B_s^0–B_s^0 system.

Using this result for mixing and our observed value of A_b^{obs} we determine $A_b = 0.130^{+0.044}_{-0.042}$ (stat) ± 0.02 (sys) and hence the effective weak mixing angle $\sin^2\bar{\theta}_W = 0.225 \pm 0.008$ (L3 1990*i*).

By comparing the number of single and double semi-leptonic decay events we observe, we can determine the b-quark semi-leptonic branching ratio. We find, $Br(b \to l + X) = 0.113 \pm 0.010$ (stat) ± 0.006 (sys), without assumptions on Γ_b. We therefore determine the partial decay width of the Z^0 into $b\bar{b}$ to be $\Gamma_b = 385 \pm 7$ (stat) ± 11 (sys) ± 19 (*Br*) (L3 1991*e*).

3.4. *QCD studies*

LEP has proven to be an excellent machine for the study of hadron physics and QCD. Due to the high energies, the quarks and gluons produced in the Z^0 decays materialize as hadrons in narrow jets with good angular separation. Since a typical $q\bar{q}$ event will give rise to two jets and a typical $q\bar{q}g$ event will have three jets; the ratio of two-jet to three-jet events can be used to determine the strong interaction coupling constant α_s. In determining the number of jets we have used the y_{cut} algorithm (JADE 1986, 1988). Effectively the value of y_{cut} determines the minimum jet energy, and hence the number of jets. A small value for y_{cut} lowers the number of multijet events but increases the separation of the jets. For a given parton recombination scheme, QCD (calculated at second order) predicts the rate of 2-, 3- and 4-jet events as a function of the parameter $\Lambda_{\overline{MS}}$, the centre of mass energy squared, $s(\approx M_Z^2)$ the scale μ^2 and the jet resolution y_{cut}. Fixing μ^2 to the central value $y_{cut}\, s$, corresponding to the typical momentum $\sqrt{(y_{cut}\, s)}$ transferred to the hard gluons radiated, and choosing the value $y_{cut} = 0.08$ where the 4-jet event rate is small, but the 3-jet event rate is still large, we obtain a value for $\Lambda_{\overline{MS}}$. This translates into α_s ($\sqrt{s} = 91.22$ GeV) $= 0.115 \pm 0.005$ (exp)$^{+0.012}_{-0.010}$ (theor) (L3 1990*j*).

We have also measured α_s from the asymmetry of the energy–energy correlations (L3 1991*f*); this method has different contributions to the theoretical uncertainty,

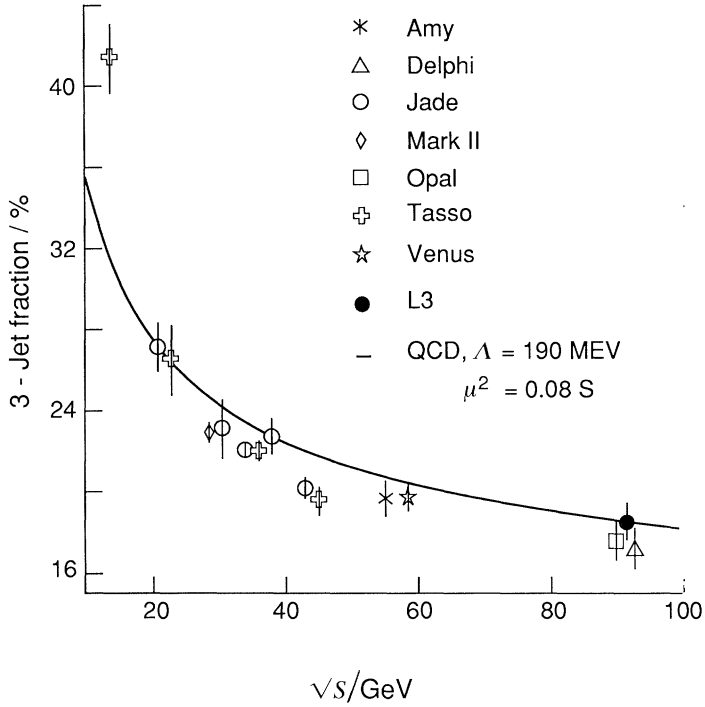

Figure 10. Energy dependence of the 3-jet fraction measured in e^+e^- annihilation at different centre of mass energies for $y_{cut} = 0.08$ in comparison with the second order QCD prediction (including hadronization effects) for $\mu^2/s = 0.08$ and our measured value of $\Lambda_{\overline{MS}}$. For a full description of the non-L3 data points, see L3 (1990*j*).

and yields consistent values for α_s. Combining all L3 measurements we obtain $\alpha_s(M_Z) = 0.115 \pm 0.01$.

In figure 10 we show the energy dependence of the 3-jet fraction at different centre of mass energies. The running of the strong interaction coupling constant can be clearly seen, as can its approach to an asymptotic value at high energy.

By selecting b-quark events as described above, we can perform the same 3-jet analysis to determine the value of α_s for b-quarks, (α_s^b). We find $\alpha_s^b/\alpha_s^{udsc} = 1.08 \pm 0.09$. Thus α_s has been found to be flavour independent within the measured uncertainties.

4. Summary

The L3 experiment has performed almost exactly as it was designed to do. We have made a large number of precision test of the Standard Model. To date, no discrepancies with the standard model have been discovered even though the precision of the tests are approaching 1%. However, the missing elements of the Standard Model such as the Higgs particle and the supersymmetric partners of the standard particles remain elusive.

The high luminosities and high energies available at LEP hold the promise of an interesting decade for experimental, and hopefully theoretical, particle physics.

I thank the Royal Society for their invitation to, and hospitality at, the meeting to which this paper was presented. The results presented here are the work of the members of the L3 Collaboration who have built and run the experiment, and have performed the analysis to obtain

the results which are presented herein. I thank the accelerator division and CERN for the remarkable way in which the LEP machine was constructed on schedule and with a performance that has almost equalled the design goals.

References

Adriani, O., *et al.* 1990 Hadron calorimetry in the L3 detector. CERN preprint CERN-PPE/90-158.

ARGUS Collaboration 1987 Observation of B^0–$\bar{B}^0$ mixing. *Phys. Lett.* B **192**, 245–252.

Berends, F. A. & Kleiss, R. 1985 Initial state radiation at LEP energies and the corrections to Higgs boson production. *Nucl. Phys.* B **260**, 32–60.

CLEO Collaboration 1989 B^0–$\bar{B}^0$ mixing at the Y (4s). *Phys. Rev. Lett.* **62**, 2233–2236.

Englert, F. & Brout, R. 1964 Broken symmetries and the mass of the gauge vector bosons. *Phys. Rev. Lett.* **13**, 321–323.

Franzini, P. J., *et al.* 1989 In Z^0 *Physics at* LEP. CERN report CERN-89-08 (ed. G. Altarelli, R. Kleiss & C. Verzegnassi), vol. II, pp. 59–119, and references therein.

Glashow, S. L. 1961 Partial symmetries of weak interactions. *Nucl. Phys.* B **22**, 579–588.

Higgs, P. W. 1964*a* Broken symmetries, massless particles and gauge fields. *Phys. Lett.* **12**, 132–133.

Higgs, P. W. 1964*b* Broken symmetries and the masses of the gauge bosons. *Phys. Rev. Lett.* **13**, 508–509.

Higgs, P. W. 1966 Spontaneous symmetry breaking without massless bosons. *Phys. Rev.* **145**, 1156–1163.

JADE Collaboration 1986 Experimental studies on multijet production in e^+e^- annihilation at PETRA energies. *Z. Phys.* C **33**, 23–31.

JADE Collaboration 1988 Experimental investigation of the energy dependence of the strong coupling strength. *Phys. Lett.* B **213**, 235–241.

L3 Collaboration 1989 A determination of the properties of the neutral intermediate vector boson Z^0. *Phys. Lett.* B **231**, 509–518.

L3 Collaboration 1989*a* Mass limits for scalar muons, scalar electrons and winos from e^+e^- collisions near $\sqrt{s} = 91$ GeV. *Phys. Lett.* B **233**, 530–537.

L3 Collaboration 1990 The construction of the L3 experiment. *Nucl. Instrum. Meth.* A **289**, 35–102.

L3 Collaboration 1990*a* Search for the neutral Higgs boson in Z^0 decay. *Phys. Lett.* B **248**, 203–210.

L3 Collaboration 1990*b* Search for a low mass Higgs boson in Z^0 decay. *Phys. Lett.* B **252**, 518–524.

L3 Collaboration 1990*c* Mass limits for excited electrons and muons from Z^0 decay. *Phys. Lett.* B **247**, 177–184.

L3 Collaboration 1990*d* Search for excited taus from Z^0 decays. *Phys. Lett.* B **250**, 205–211.

L3 Collaboration 1990*e* Search for the neutral Higgs boson of the minimal supersymmetric standard model from Z^0 decays. *Phys. Lett.* B **251**, 311–320.

L3 Collaboration 1990*f* A search for heavy charged and neutral leptons from Z^0 decays. *Phys. Lett.* B **252**, 321–330.

L3 Collaboration 1990*g* Search for excited neutrinos from Z^0 decays. *Phys. Lett.* B **252**, 525–532.

L3 Collaboration 1990*h* A measurement of B^0–$\bar{B}^0$ mixing in Z^0 decays. *Phys. Lett.* B **252**, 703–712.

L3 Collaboration 1990*i* A measurement of the $Z^0 \to b\bar{b}$ forward–backward asymmetry. *Phys. Lett.* B **252**, 713–721.

L3 Collaboration 1990*j* Determination of α_s from jet multiplicities measured on the Z^0 resonance. *Phys. Lett.* B **248**, 464–472.

L3 Collaboration 1991 A measurement of the average lifetime of B-hadrons. L3 Preprint 31. (In preparation.)

L3 Collaboration 1991*a* Measurement of electroweak parameters from hadronic and leptonic decays of the Z^0. L3 Preprint 28, 15 February 1991.

PHILOSOPHICAL TRANSACTIONS OF THE ROYAL SOCIETY A MATHEMATICAL, PHYSICAL & ENGINEERING SCIENCES

L3 Collaboration 1991*b* Search for the neutral Higgs boson. *Phys. Lett.* B **257**, 450–458.

L3 Collaboration 1991*c* Search for leptoquarks in Z^0 decay. L3 Preprint 26, 1 March 1991.

L3 Collaboration 1991*d* Search for high-mass resonances in radiative decays of the Z^0. L3 Preprint 29, 28 February 1991.

L3 Collaboration 1991*e* Measurement of $Z^0 \rightarrow b\bar{b}$ decays and the semileptonic branching ratio $Br(b \rightarrow l + X)$, L3 Preprint 27, 18 February, 1991.

L3 Collaboration 1991*f* Determination of α_s from energy–energy correlations measured on the Z^0 resonance. *Phys. Lett.* B **257**, 469–478.

Salam, A. 1968 Weak and electromagnetic interactions. In *Elementary particle theory* (ed. N. Svartholn), pp. 367–377. Stockholm: Almquist and Wiskell.

UA1 Collaboration 1987 Search for B^0–$\bar{B}^0$ oscillations at the CERN proton–antiproton collider. *Phys. Lett.* B **186**, 247–254; Errata. *Phys. Lett.* B **197**, 565.

Weinberg, S. 1967 A model of leptons. *Phys. Rev. Lett.* **19**, 1264–1266.

PHILOSOPHICAL TRANSACTIONS OF THE ROYAL SOCIETY A MATHEMATICAL, PHYSICAL & ENGINEERING SCIENCES

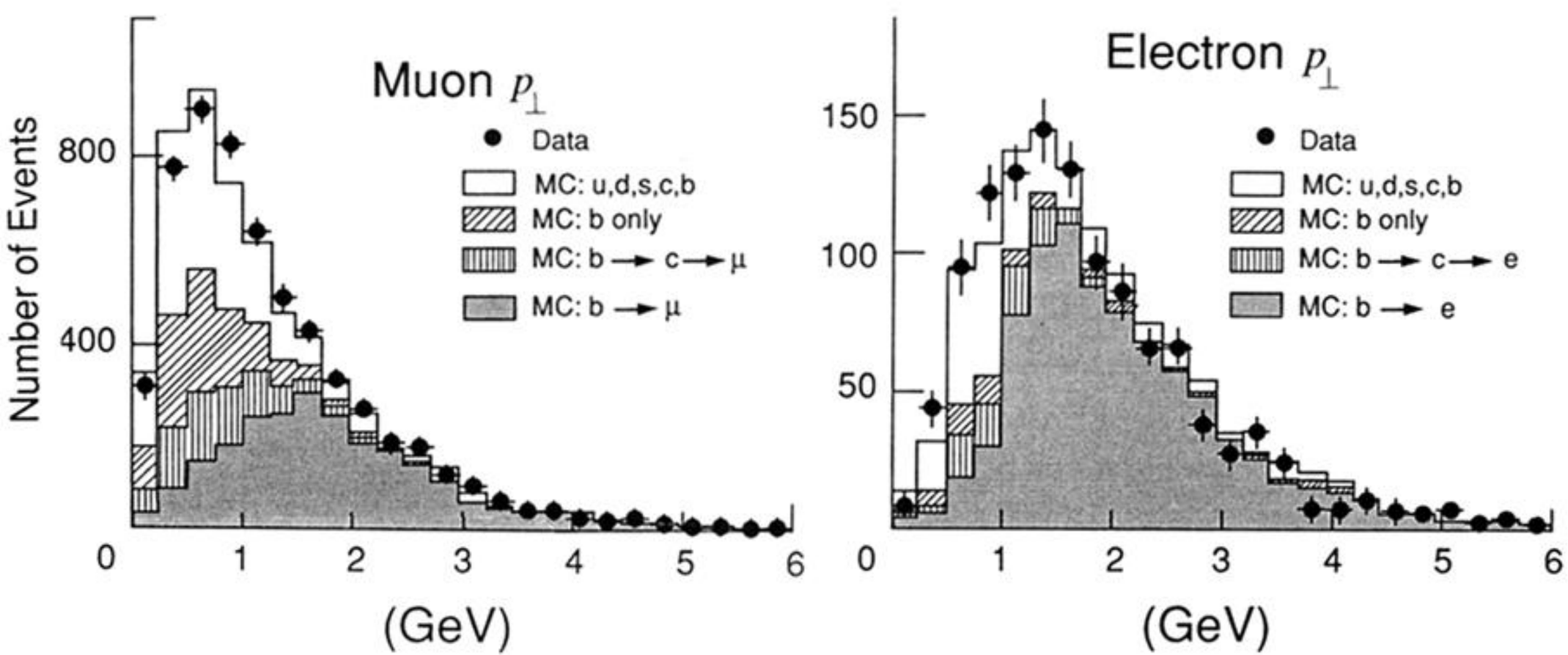

igure 9. The measured distributions of the transverse momentum $p_\perp$ of the muon (a) and electron) with respect to the nearest jet. Cuts of $P_\mu > 4$ GeV for the muons and $P_e > 3$ GeV for the ectrons have been applied. The contributions of the various processes are indicated. The data at rge $p_\perp$ are dominated by b → l decays.